

Quantifying uncertainty in lung cancer segmentation with foundation models applied to mixed-domain datasets

Aneesh Rangnekar^a, Nishant Nadkarni^a, Jue Jiang^a, and Harini Veeraraghavan^a

^aDepartment of Medical Physics, Memorial Sloan Kettering Cancer Center, NY, USA

ABSTRACT

Medical image foundation models have shown the ability to segment organs and tumors with minimal fine-tuning. These models are typically evaluated on task-specific in-distribution (ID) datasets. However, reliable performance on ID dataset does not guarantee robust generalization on out-of-distribution (OOD) datasets. Importantly, once deployed for clinical use, it is impractical to have ‘ground truth’ delineations to assess ongoing performance drifts, especially when images fall into OOD category due to different imaging protocols. Hence, we introduced a comprehensive set of computationally fast metrics to evaluate the performance of multiple foundation models (Swin UNETR, SimMIM, iBOT, SMIT) trained with self-supervised learning (SSL). SSL pretraining was selected as this approach is applicable for large, diverse, and unlabeled image sets. All models were fine-tuned on identical datasets for lung tumor segmentation from computed tomography (CT) scans. SimMIM, iBOT, and SMIT used identical architecture, pretraining, and fine-tuning datasets to assess performance variations with the choice of pretext tasks used in SSL. Evaluation was performed on two public lung cancer datasets (LRAD: $n = 140$, 5Rater: $n = 21$) with different image acquisitions and tumor stage compared to training data ($n = 317$ public resource with stage III-IV lung cancers) and a public non-cancer dataset containing volumetric CT scans of patients with pulmonary embolism ($n = 120$). All models produced similarly accurate tumor segmentation on the lung cancer testing datasets. SMIT produced a highest F1-score (LRAD: 0.60, 5Rater: 0.64) and lowest entropy (LRAD: 0.06, 5Rater: 0.12), indicating higher tumor detection rate and confident segmentations. In the OOD dataset, SMIT misdetected least number of tumors, indicated by median volume occupancy of 5.67 cc compared to second best method SimMIM of 9.97 cc. Our analysis shows that additional metrics such as entropy and volume occupancy may help to better understand model performance on mixed domain datasets.

Keywords: Lung cancer, in-distribution, out-of-distribution, segmentation, foundation models, CT

1. PURPOSE/MOTIVATION

Foundation models are developed with the ultimate goal of universal applicability to a variety of problems with minimal fine-tuning to new tasks. Once fine-tuned, these models are evaluated on selected in-domain datasets with similar distribution as the fine-tuning datasets, using task-specific accuracy metrics. However, task-specific metrics may not be sufficient to ensure reliably accurate performance when such models are to be deployed for multi-institutional research or routine clinical use, where datasets can exhibit wide variations from training data. Performance drift occurs when test image distribution diverges from the training distribution, a challenge known as distribution shift. Another source of poor performance is from concept drift when the datasets used in broader testing have diseases that differ from those used in training data (e.g. data trained on advanced stage malignant cancers applied to segment precancerous or early stage cancers or on non-cancer datasets). Models must be resilient to image distribution shifts and concept drifts.

Currently, a segmentation model’s performance is quantified only using segmentation metrics, which provides a limited view of robustness in out-of-domain datasets. Out-of-distribution (OOD) analysis is routinely done in computer vision applications that systematically computes OOD performance metrics in addition to task-specific accuracy metrics;¹ OOD metrics are not often used for analysis in medical image segmentations.^{2,3} Hence we extended OOD metrics used in natural image analysis to evaluate OOD performance and also quantify uncertainty in the medical image segmentation applicable to cases with distribution and concept shifts. We

Further author information: Send correspondence to A. Rangnekar at rangnea@mskcc.org

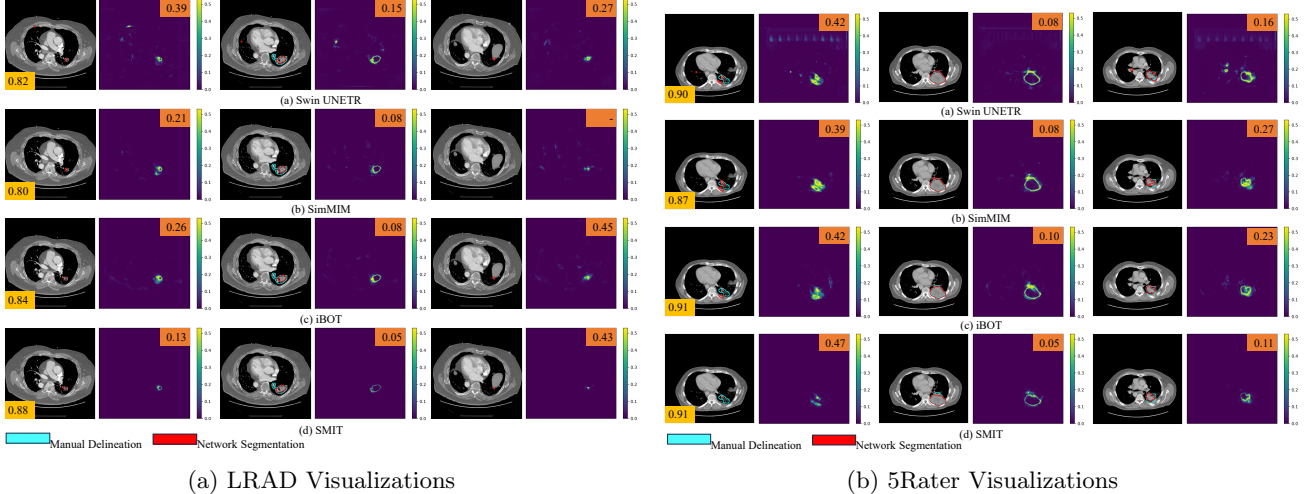


Figure 1: Example segmentations and voxel-wise entropy shown for superior, central, and inferior slices. Average entropy for individual slices is shown on top-right. Volumetric DSC for the entire image is shown in yellow on the bottom-left. The ‘-’ indicates that the model did not detect/segment any tumor.

systematically evaluated four different foundation models for generating volumetric lung tumor segmentation from contrast and non-contrast 3D-CTs. Lung tumor segmentation was selected as this is more complex than organ segmentation and multiple public benchmarking CT thoracic datasets are available to assess accuracy with both distribution and concept drifts.

2. METHODS

Foundation Models: Swin UNETR,^{4,5} SimMIM,⁶ iBOT⁷ and SMIT,⁸ trained on the 3D-Swin transformer backbone in order to use a consistent network backbone, were used in this study. Also, SimMIM, iBOT, and SMIT used identical encoder and decoder architecture, consistent data augmentations, and standardized training hyperparameters. Our purpose for maintaining architecture similarity was to answer: *how do pretraining tasks affect downstream performance and can we quantify performance differences?*

SimMIM uses masked image pretask that applies a random mask to the input (in our case, 3D mask to a 3D cube) and then trains the neural network to reconstruct the masked regions. This approach encourages the model to learn contextual information as it has to rely on the visible parts to predict the missing regions. iBOT extends SimMIM by learning to good feature representations from masked regions via token distillation in a teacher-student framework. iBOT uses a combination of local (voxel-level) and global (scan-level) tokens for pretraining the network. SMIT combines the masked image modeling and token distillation used in SimMIM and iBOT to learn dense pixel dependencies with iBOT’s local-global connections. For all our models, we used a Swin transformer with depth of 2 – 2 – 12 – 2 and an input size of $128 \times 128 \times 128$. We used the decoder heads as mentioned in the corresponding literature for pretraining and used a consistent U-Net decoder initialized with random weights for the fine-tuning. Swin UNETR⁴ model pretrained weights and model structure (depth of 2 – 2 – 2 – 2 and an input size of $96 \times 96 \times 96$) were used as is to maintain consistency with the published work.

Pretraining Datasets: We used 10,412 3D CT scans encompassing diseases from head and neck to the pelvis sourced from datasets provided publicly for variety of tasks including lesion detection,⁹ classification,¹⁰ and multi-organ and abdominal tumor segmentations for pretraining. Anonymized institutional 3D-CT datasets from patients treated for lung, esophageal, and head and neck cancers with radiation were used as is without any curation. **Fine-tuning** was performed using public dataset containing stage III-IV non-small cell lung cancers (NSCLC) ($n = 317$ 3D-CTs), with a 70%-30% stratified training and validation split.¹¹ **Testing datasets:** Two in-distribution (ID) with same concept but different CT acquisitions (distribution shift) were evaluated. This included patients with early stage I-II NSCLC¹² (referred to as LRAD) and stage II-IV with multi-rater segmentations¹³ (referred to as 5Rater). Last, one OOD dataset (concept drift) consisting of a subset of 120 annotated

Table 1: Fine-tuned foundation model performances on the ID datasets. The entropy values for the values for validation set are as follows: Swin UNETR: 0.17 ± 0.06 , SimMIM: 0.15 ± 0.06 , iBOT: 0.17 ± 0.06 , SMIT: 0.07 ± 0.03 .

Pretraining Strategy	LRAD Dataset (N = 140)				5Rater Dataset (N = 21)			
	DSC	HD95 (mm)	F1-Score	Entropy	DSC	HD95 (mm)	F1-Score	Entropy
Swin UNETR ⁴	0.78 ± 0.09	6.71 ± 7.89	0.481	0.20 ± 0.07	0.86 ± 0.01	5.10 ± 7.77	0.416	0.19 ± 0.05
SimMIM ⁶	0.80 ± 0.07	5.09 ± 4.61	0.553	0.16 ± 0.06	0.83 ± 0.14	4.65 ± 7.59	0.466	0.21 ± 0.06
iBOT ⁷	0.80 ± 0.08	5.53 ± 5.24	0.555	0.16 ± 0.07	0.87 ± 0.06	3.35 ± 4.00	0.353	0.23 ± 0.06
SMIT ⁸	0.81 ± 0.07	5.39 ± 5.07	0.601	0.06 ± 0.04	0.86 ± 0.06	4.43 ± 5.51	0.641	0.12 ± 0.06

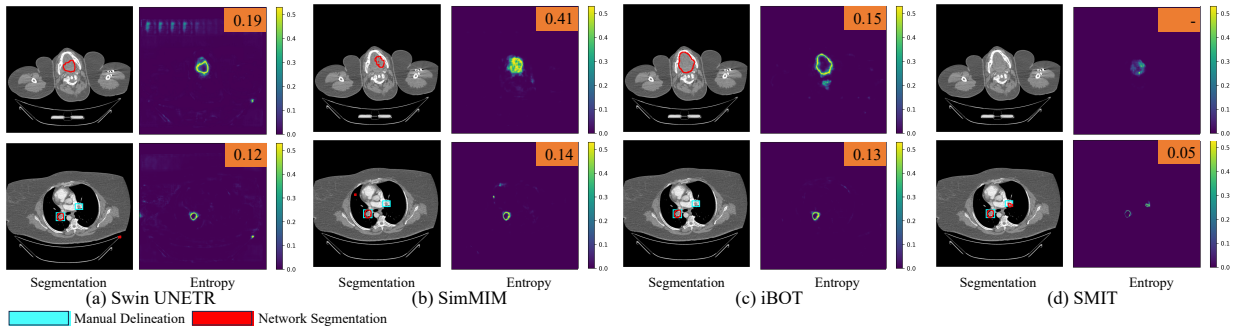


Figure 2: Example segmentations and corresponding entropy for the four models on 3 different images from the Pulmonary Embolism dataset. The slice-wise entropy is displayed in orange on top-right. The ‘-’ indicates that the model did not detect/segment any tumor.

images from the RSNA Pulmonary Embolism (PEmb) dataset^{14,15} was evaluated to assess robustness to false detections. The OOD dataset presents an additional challenge as the disease occurs in the same anatomical region (chest CT) as used for training and are confirmed to be devoid of cancers.

Implementation details: Models were fine-tuned using Dice and Cross-Entropy losses with a batch size of 16 (4×4 NVIDIA A100 GPUs), learning rate of $2e^{-4}$, and linear warmup scheduler with cosine annealing for 1000 epochs (with Pytorch¹⁶). The lung window of $[-400, 400]$ HU and $1mm \times 1mm \times 1mm$ voxel spacing was used throughout all experiments. Sliding window inference with 50% Gaussian overlap to segment volumetric CTs with varying fields of view.^{4,8}

Segmentation metrics: Dice similarity coefficient (**DSC**) and Hausdorff distance at 95th percentile (**HD95**) computes the volumetric dice and distance for clustered tumor regions where the 3D overlap between manual delineations and predicted segmentations is $\geq 50\%$. **F1-score** was computed as a combination of precision and recall to measure the total number of clustered regions that were incorrectly identified as tumors or completely missed by the algorithm, respectively.

OOD metrics: Tumor segmentation is binary voxel-wise classification. Voxels that were classified as tumor (class = 1) were used in the computation and averaged to extract the following image-level OOD metrics: **AUROC** or area under the receiver operating curve, measures the accuracy of correctly identifying an image as an example from the OOD dataset. **FPR@95** represents the false positive rate of the binary classifier at the 95% decision threshold, wherein it measures how often a model mistakenly labels an ID image as OOD when the model correctly identifies 95% of the OOD examples. Effectively, it rates the confidence of the model predictions. **Entropy** quantifies the uncertainty in the model’s tumor predictions, providing a different insight on the confidence of the model about its classification. Higher entropy indicates the model has encountered data from an unfamiliar distribution and is less certain of its predictions. **Volume occupancy** measures the total misdetected tumor volume (in cc). This metric quantifies the actual number of voxels that were incorrectly segmented instead of averaging metrics across an entire image.

3. RESULTS

As shown in Table 1, all models produced similarly accurate tumor segmentations in both datasets. However, SMIT produced a higher F1 score, indicating higher precision and recall rate. It was also more confident

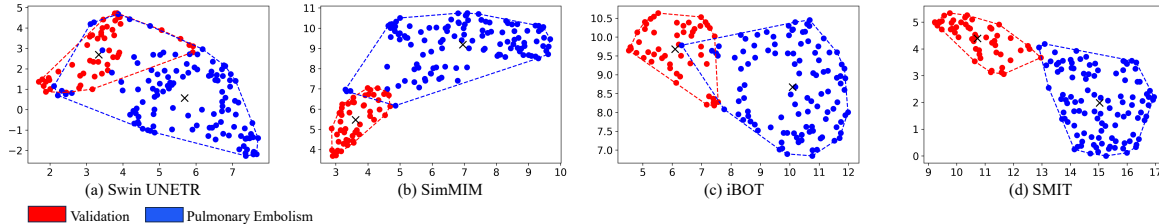


Figure 3: UMAP clustering for features of the validation and Pulmonary Embolism images derived from Stage 1 of the Swin transformer architecture for all four foundation models.

Table 2: OOD Detection performance of the foundation models post fine-tuning. We report results using Maximum Softmax Probability for AUROC and FPR95 and report the Volume Occupancy as median and inter-quartile range.

Pretraining Strategy	Pulmonary Embolism Dataset (N = 120)			
	Volume Occupancy (cc)	Entropy	AUROC	FPR@95
Swin UNETR ⁴	16.24 [4.56 ± 75.58]	0.27 ± 0.05	90.77	26.92
SimMIM ⁶	9.97 [1.03 ± 55.71]	0.26 ± 0.07	91.65	23.53
iBOT ⁷	8.46 [0.55 ± 98.24]	0.27 ± 0.08	88.12	42.31
SMIT ⁸	5.67 [0.56 ± 37.75]	0.15 ± 0.06	89.58	34.62

compared to other methods as shown by the lowest average entropy. Of the compared methods, SwinUNETR was the least accurate and had the highest entropy. Figures 1a and 1b show segmentation and voxel-wise entropy for representative examples produced by all methods for superior, central, and inferior tumor extent slices. SMIT consistently had higher uncertainty at the boundary compared to other models that also showed higher entropy inside the tumor. Entropy is expected to be higher at the boundary due to tumor and healthy tissue interface.

Table 2 presents the results for OOD detection. As shown, SimMIM had the best OOD performance in terms of AUROC and FPR@95 metrics. SMIT had slightly lower AUROC and FP@95 compared to SimMIM but lower entropy, indicating that this network produced confident incorrect predictions. On the other hand, SMIT also resulted in the least number of voxels being misclassified as tumors compared to all other methods. Figure 2 shows that all models except SMIT falsely segment a tumor in the oral cavity in the first case. SMIT did not generate a segmentation, although uncertainty that is lower than all the other models is indicated. In the second case (bottom row), SMIT segmented both the embolisms identified by radiologists. SwinUNETR, SimMIM, and iBOT identified one of the two embolisms and also generated false detections (table for SwinUNETR, top right lung region for SimMIM). Detecting pulmonary embolisms as tumors presents a dual challenge of zero-shot detection as well as conservative prediction, both of which are beyond the current scope of this paper.

To further analyze the contribution of features towards OOD performance, we computed unsupervised clustering of the stage I features extracted by the transformer networks.¹⁷ Features were extracted by randomly sampling two $128 \times \times 3D$ crops containing the segmented tumors (centered on the tumor wherever applicable), taking an average representation of the voxels and then applying UMAP with $n.neighbors = 20$, $min.dist = 0.1$, and the Euclidean metric for distance.. UMAP¹⁸ cluster results are shown in Figure 3. As shown, there was a lot of overlap between the tumor and pulmonary embolism features for Swin UNETR and iBOT networks. SMIT and SimMIM were able to better differentiate the two datasets, indicating that feature representations extracted by these networks are more robust to OOD variations.

4. CONCLUSION

We performed a comprehensive evaluation of robustness of foundation models applied to lung cancer segmentation. Our analysis showed that whereas the models can exhibit similar volumetric segmentation accuracy, analysis of entropy as well as out of distribution robustness metrics, such as mis-detected tumor volume occupancy, provides a more comprehensive perspective on model performance. Our analysis shows that metrics combining OOD performance with task-specific metrics provides us valuable insights into understanding model behavior when deploying in clinical settings, where the ground-truth labels are often unknown.

ACKNOWLEDGMENTS

This research was partially supported by NCI R01CA258821 and Memorial Sloan Kettering (MSK) Cancer Center Support Grant/Core Grant NCI P30CA008748.

REFERENCES

- [1] Yang, J., Zhou, K., Li, Y., and Liu, Z., “Generalized out-of-distribution detection: A survey,” *International Journal of Computer Vision*, 1–28 (2024).
- [2] Graham, M. S., Tudosiu, P.-D., Wright, P., Pinaya, W. H. L., Jean-Marie, U., Mah, Y. H., Teo, J. T., Jager, R., Werring, D., Nachev, P., et al., “Transformer-based out-of-distribution detection for clinically safe segmentation,” in [*International Conference on Medical Imaging with Deep Learning*], 457–476, PMLR (2022).
- [3] Yuan, M., Xia, Y., Dong, H., Chen, Z., Yao, J., Qiu, M., Yan, K., Yin, X., Shi, Y., Chen, X., et al., “Devil is in the queries: Advancing mask transformers for real-world medical image segmentation and out-of-distribution localization,” in [*Proceedings of the IEEE/CVF Conference on Computer Vision and Pattern Recognition*], 23879–23889 (2023).
- [4] Tang, Y., Yang, D., Li, W., Roth, H. R., Landman, B., Xu, D., Nath, V., and Hatamizadeh, A., “Self-supervised pre-training of swin transformers for 3d medical image analysis,” in [*Proceedings of the IEEE/CVF Conference on Computer Vision and Pattern Recognition*], 20730–20740 (2022).
- [5] Willeminck, M., Roth, R., and Sandfort, V., “Toward foundational deep learning models for medical imaging in the new era of transformer networks,” *Radiol Artif Intell* **4**(6) (2022).
- [6] Xie, Z., Zhang, Z., Cao, Y., Lin, Y., Bao, J., Yao, Z., Dai, Q., and Hu, H., “Simmm: A simple framework for masked image modeling,” in [*Proceedings of the IEEE/CVF conference on computer vision and pattern recognition*], 9653–9663 (2022).
- [7] Zhou, J., Wei, C., Wang, H., Shen, W., Xie, C., Yuille, A., and Kong, T., “ibot: Image bert pre-training with online tokenizer,” *arXiv preprint arXiv:2111.07832* (2021).
- [8] Jiang, J., Tyagi, N., Tringale, K., Crane, C., and Veeraraghavan, H., “Self-supervised 3d anatomy segmentation using self-distilled masked image transformer (smit),” in [*International Conference on Medical Image Computing and Computer-Assisted Intervention*], 556–566, Springer (2022).
- [9] Xiao, Y., Yang, G., and Song, S., [*Lesion Segmentation in Surgical and Diagnostic Applications: MICCAI 2022 Challenges, CuRIOUS 2022, KiPA 2022 and MELA 2022, Held in Conjunction with MICCAI 2022, Singapore, September 18–22, 2022, Proceedings*], vol. 13648, Springer Nature (2023).
- [10] Harmon, S. A., Sanford, T. H., Xu, S., Turkbey, E. B., Roth, H., Xu, Z., Yang, D., Myronenko, A., Anderson, V., Amalou, A., et al., “Artificial intelligence for the detection of covid-19 pneumonia on chest ct using multinational datasets,” *Nature communications* **11**(1), 4080 (2020).
- [11] Aerts, H., Velazquez, E. R., Leijenaar, R., Parmar, C., Grossmann, P., Cavalho, S., Bussink, J., Monshouwer, R., Haibe-Kains, B., Rietveld, D., et al., “Data from nsclc-radiomics,” *The cancer imaging archive* (2015).
- [12] Bakr, S., Gevaert, O., Echegaray, S., Ayers, K., Zhou, M., Shafiq, M., Zheng, H., Zhang, W., Leung, A., Kadoch, M., et al., “Data for nsclc radiogenomics collection,” *The Cancer Imaging Archive* **10**, K9 (2017).
- [13] Wee, L., Aerts, H., Kalendralis, P., and Dekker, A., “Data from NSCLC-Radiomics-Interobserver1 [data set],” (2019).
- [14] Colak, E., Kitamura, F. C., Hobbs, S. B., Wu, C. C., Lungren, M. P., Prevedello, L. M., Kalpathy-Cramer, J., Ball, R. L., Shih, G., Stein, A., et al., “The rsna pulmonary embolism ct dataset,” *Radiology: Artificial Intelligence* **3**(2), e200254 (2021).
- [15] Callejas, M. F., Lin, H. M., Howard, T., Aitken, M., Napoleone, M., Jimenez-Juan, L., Moreland, R., Mathur, S., Deva, D. P., and Colak, E., “Augmentation of the rsna pulmonary embolism ct dataset with bounding box annotations and anatomic localization of pulmonary emboli,” *Radiology: Artificial Intelligence* **5**(3), e230001 (2023).
- [16] Paszke, A., Gross, S., Massa, F., Lerer, A., Bradbury, J., Chanan, G., Killeen, T., Lin, Z., Gimelshein, N., Antiga, L., et al., “Pytorch: An imperative style, high-performance deep learning library,” *Advances in neural information processing systems* **32** (2019).

- [17] Masarczyk, W., Ostaszewski, M., Imani, E., Pascanu, R., Miłoś, P., and Trzcinski, T., “The tunnel effect: Building data representations in deep neural networks,” *Advances in Neural Information Processing Systems* **36** (2024).
- [18] McInnes, L., Healy, J., Saul, N., and Großberger, L., “Umap: Uniform manifold approximation and projection,” *Journal of Open Source Software* **3**(29), 861 (2018).